

Electronic Supplementary Information

Stackable bipolar pouch cells with corrosion-resistant current collectors enable high-power aqueous electrochemical energy storage

Brian Evanko,^{#ab} Seung Joon Yoo,^{*#b} Jason Lipton,^c Sang-Eun Chun,^d Martin Moskovits,^c Xiulei Ji,^e Shannon W. Boettcher,^{*f} and Galen D. Stucky^{ac}

^a *Materials Department, University of California, Santa Barbara, California 93106, USA*

^b *Materials Research Laboratory, University of California, Santa Barbara, California, 93106, USA. E-mail: sjyoo@chem.ucsb.edu*

^c *Department of Chemistry & Biochemistry, University of California, Santa Barbara, California 93106, USA*

^d *School of Materials Science and Engineering, Kyungpook National University, Daegu 41566, Republic of Korea*

^e *Department of Chemistry, Oregon State University, Corvallis, Oregon 97331, USA*

^f *Department of Chemistry & Biochemistry, University of Oregon, Eugene, Oregon 97403, USA. E-mail: swb@uoregon.edu*

These authors contributed equally to this work.

Resistivity/Conductivity Calculations (Fig. 2c)

In order to calculate current collector (CC) requirements for an idealized monopolar cell architecture, we devised a model corresponding to the diagram in Fig. S1a. It is assumed that the current density, J , across the electrode-CC interface is uniform over the entire cell and that a continuous, highly conductive tab runs across the entire top of the CC to connect it to the device terminals. In an actual cell, tabbing is unlikely to be continuous and there will also be a voltage gradient within the CC that causes higher current densities near the tabs and lower current densities further from the tabs. However, in the high-rate charge-discharge condition discussed in this work, current density is most likely to be limited by the resistance and kinetics of the electrolyte and electrode. For this reason, the uniform current density assumption is reasonable for a first-order analysis and allows one to make a simple estimate of CC resistivity and thickness requirements.

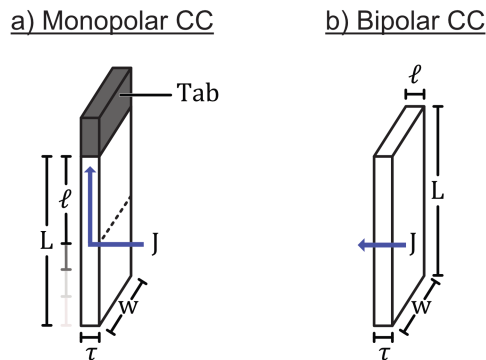


Fig. S1 Simplified schematic of monopolar and bipolar current collectors. The parameters for estimating the IR drop in (a) a monopolar CC and (b) a bipolar CC. The CC dimensions for both schematics are the height, L , the width, w , and the thickness, τ . The current density, J , across the electrode/CC interface is uniform at all points, and ℓ indicates the possible path lengths current can travel between the tab and the different points where it enters the CC. For example, ℓ is variable for the monopolar cell, ranging from $\ell = 0$ to $\ell = L$, but constant in the bipolar cell ($\ell = \tau$).

The monopolar CC dimensions shown in Fig. S1a are its height, L , measured perpendicular to the tab, its width, w , measured parallel to the tab, and its thickness, τ . In this configuration current must flow different distances, ℓ , from the points where it enters the CC to the tab. In the CC there is a fixed resistivity, ρ , and the current flows through a cross-sectional area, A , where $A = w \cdot \tau$. The contribution to the IR drop that is attributed to the monopolar current collector (dV_{MCC}) for each value of ℓ is calculated by using the following equation:

$$dV_{\text{MCC}} = dI \cdot R_{\text{MCC}}(\ell)$$

Here R_{MCC} is the sheet resistance of the current collector at a distance ℓ from the tab and dI is the current entering the CC at this distance. It is possible to express these values in terms of ℓ :

$$dI = J \cdot w \cdot d\ell$$

$$R_{\text{MCC}} = \frac{\rho \cdot \ell}{A} = \frac{\rho \cdot \ell}{w \cdot \tau}$$

Combining these equations gives:

$$dV_{\text{MCC}} = J \cdot w \cdot d\ell \cdot \frac{\rho \cdot \ell}{w \cdot \tau} = J \cdot \frac{\rho \cdot \ell}{\tau} d\ell$$

This equation is then integrated over the entire CC length to obtain the total voltage drop across the entire current collector with height L :

$$V_{\text{MCC}} = \int_0^L J \cdot \frac{\rho \cdot \ell}{\tau} d\ell = \frac{J \cdot \rho \cdot L^2}{2\tau}$$

Finally, for the full cell, the IR drop at the transition from charge to discharge (ΔV_{MCC}) is calculated by using $\Delta J = J_{\text{ch}} - J_{\text{dis}}$. The value for ΔV_{MCC} is doubled to account for two electrodes and CCs in each cell:

$$\Delta V_{\text{MCC}} = \frac{\Delta J \cdot \rho \cdot L^2}{\tau}$$

We note that this relationship assumes that electrodes are coated onto only one side of the monopolar CC. Double-sided coating would double dI and place more demanding requirements on CC materials.

The IR drop calculation was repeated for bipolar CCs. The bipolar CC dimensions shown in Fig. S1b are again the height, L , the width, w , and the thickness, τ . The current density, J ,

across the entire electrode-CC interface is uniform over the entire cell at all conditions for a bipolar cell. In this configuration current flows in the through-plane direction over a distance ℓ , where $\ell = \tau$. In the CC there is a fixed resistivity, ρ , and the current flows through a cross-sectional area, A , where $A = w \cdot L$. The contribution to the IR drop that is attributed to the bipolar current collector (V_{BCC}) is calculated with the following equation:

$$V_{\text{BCC}} = I \cdot R_{\text{BCC}}$$

Here R_{BCC} is the resistance of the bipolar current collector and I is the current passing through the CC. It is possible to express these values alternately as:

$$I = J \cdot w \cdot L$$

$$R_{\text{BCC}} = \frac{\rho \cdot \ell}{A} = \frac{\rho \cdot \tau}{w \cdot L}$$

Combining these equations gives:

$$V_{\text{BCC}} = J \cdot w \cdot L \cdot \frac{\rho \cdot \tau}{w \cdot L} = J \cdot \rho \cdot \tau$$

Finally, for the full cell, the IR drop at the transition from charge to discharge (ΔV_{BCC}) is calculated by using $\Delta J = J_{\text{ch}} - J_{\text{dis}}$. The value for V_{BCC} is doubled to account for two electrodes and CCs per cell, then halved to account for each CC being shared between two cells:

$$\Delta V_{\text{BCC}} = \Delta J \cdot \rho \cdot \tau$$

In the manuscript, the derived equations for ΔV_{MCC} and ΔV_{BCC} are used to calculate the maximum resistivity, ρ , that a monopolar or bipolar CC material could have (while maintaining an IR drop less than ΔV_{CC} at a current density of ΔJ) as a function of cell height, L , for a variety of thicknesses, τ . For example, for a cell size of 5 cm with 50- μm -thick current collectors we can apply the condition that the CC IR drop contribution be less than 100 mV at a current density of $\pm 100 \text{ mA cm}^{-2}$. Using the equations for ΔV_{MCC} and ΔV_{BCC} with these values we find that for a monopolar cell the highest acceptable value for ρ is $1.0 \times 10^{-4} \Omega\text{-cm}$ and that for a bipolar cell the highest acceptable value for ρ is a substantially higher 100 $\Omega\text{-cm}$.

Cost Estimates

Previous studies have compared the relative price of 200- μm -thick sheets of different current collector materials offered in small quantities from specialty suppliers.^{1,2} Due to the different cell architecture in this work, we performed a comparison looking at the *thinnest mass produced foil or film of each material* instead of comparing on a constant-thickness basis. For stainless steel, nickel, and titanium foils this thickness is 25 μm (1 mil), while aluminum foil for battery applications is 15 μm thick. For carbon materials, the thinnest expanded graphite, CBPE, and pyrolytic graphite foils are 130 μm , 70 μm , and 50 μm , respectively. The properties of these materials are summarized in Table S1. While lower thicknesses are available for some specialty materials, they are not available in large quantities and tend to be too expensive for use in battery applications.

Table S1. Resistivity of metallic and carbon-based candidate current collectors

	Material	Thickness (μm)	Density (g cm^{-3})	Areal mass (mg cm^{-2})	Cost ($\text{\\$ m}^{-2}$)	Resistivity ($\Omega\text{-cm}$)
METALS	Aluminum Foil*	15	2.7	4.1	0.6	2.8×10^{-6}
	316L Stainless Steel (SS)	25	8.1	20.3	1.6	7.4×10^{-5}
	Nickel	25	8.9	22.3	7.8	7.0×10^{-6}
	Titanium	25	4.5	11.3	6.2	4.2×10^{-5}
CARBONS	Expanded Graphite (EG)	130	1.12	14.6	0.9	8.0×10^{-4}
	Pyrolytic Graphite (PG)	50	2.1	10.5	10.5	1×10^{-4}
	CBPE	70	1.15	8.1	1.6	3.5

*Non-aqueous cells only – included for reference

Reliable data on production *costs* of these materials are difficult to find, so we instead made our best effort to find bulk *pricing* for large rolls ($> 10 \text{ m}^2$) and assumed that pricing reflects a 15% markup over cost. The pricing data for CBPE came directly from the manufacturer's website (Caplinq.com). Pricing data for other materials came from Alibaba.com, Allfoils.com, and Graphitematerials.com. There was a large variation in price for the more expensive materials (titanium, nickel, and pyrolytic graphite) and a smaller variation in price for the cheaper materials (expanded graphite, stainless steel, and CBPE), so a $\pm 20\%$ uncertainty is assumed for each material. The areal cost and mass for each material are summarized in Fig. S2.

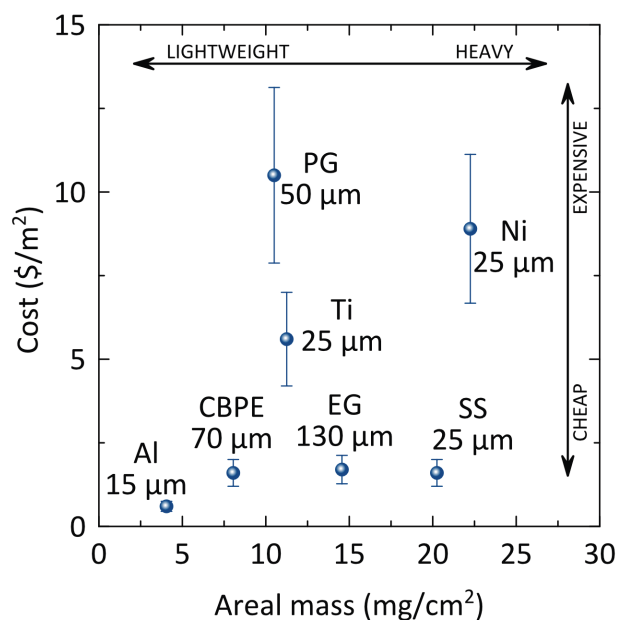


Fig. S2 Areal mass and cost for several metallic and carbon-based current collectors. Materials shown are based on the thinnest mass-produced foil or sheet available. Although aluminum is unsuitable for aqueous systems, it is shown for reference to indicate the typical mass and cost for a current collector in a non-aqueous energy storage device. EG = expanded graphite, PG = pyrolytic graphite, SS = 316L stainless steel.

Experimental Information

Chemicals. All reagents and starting materials were obtained commercially and used as received without any further purification.

Sodium bromide (NaBr), sodium sulfate (Na₂SO₄), potassium hydroxide (KOH), and tetrabutylammonium bromide (TBABr) were purchased from Sigma-Aldrich. Zinc bromide (ZnBr₂) and sodium chloride (NaCl) were purchased from Fisher Chemical. Sulfuric acid (H₂SO₄) was purchased from EMD Millipore Corporation. Poly(ethylene glycol) was purchased from Aldrich Chemical Company, Inc. Norit[®] A Supra activated carbon was purchased from Acros Organics. Hydrobromic acid (HBr) was purchased from Acros Organics. The carbon black/polyethylene composite (CBPE) was purchased from Caplinq (Linqstat XVCF). Expanded graphite foil was purchased from Alfa Aesar. Water was from a Milli-Q Simplicity[™] 185 system with resistivity ≥ 18.2 M Ω -cm (if not specified, all solutions in the SI and text refer to aqueous solutions).

Linear sweep voltammetry (Fig. 1). The linear sweep voltammetry experiments were carried out on a Bio-logic VMP3 potentiostat/galvanostat with a conventional three-electrode cell. Test electrolytes included 1 M Na₂SO₄, 1 M H₂SO₄, 1 M NaCl, and 1 M KOH. The reference electrode was Ag/AgCl (CH Instruments, 1 M KCl internal filling solution) for all electrolytes except KOH, which used an Hg/HgO reference electrode (1 M KOH internal filling solution). Candidate current collector materials including 316L stainless steel foil (ESPI Metals KNC7823), nickel foil (MTI EQ-PLIB-NTAB), titanium foil (STREM Chemicals 93-244), and CBPE (Linqstat XVCF) were used as working electrodes. These electrodes were masked with electrochemical tape (3M-484) to expose only a circular 6-mm-diameter area to the electrolyte. To minimize the effect of *IR* drop from poor in-plane conductivity for tests with CBPE, the side of the film not in contact with the electrolyte was laminated to roughened copper foil with conductive carbon grease (MG Chem 847-25ML conductive assembly paste).

Before each experiment, the masked working electrode was rinsed with isopropanol and then water, and the Pt wire counter electrode was rinsed with acetone followed by water. Test solutions were purged with N₂ for 10 min prior to each measurement. Cathodic sweeps were performed from the open circuit potential (E_{OC}) to -2.5 V and anodic sweeps were performed from E_{OC} to 2.5 V. The potential sweeps terminated early if a cutoff condition of 0.5 mA (1.77 mA cm⁻²) was reached. For each working electrode/electrolyte combination, three cathodic sweeps were performed first, followed by three anodic sweeps. The third sweeps have been plotted for comparison.

Cyclic Voltammetry. The cyclic voltammetry (CV) experiment for zinc deposition and stripping was carried out in a conventional three electrode cell with a CBPE working electrode (as described in the previous section), a Pt wire counter electrode, and an Ag/AgCl reference electrode (CH Instruments). The test solution of 0.1 M ZnBr₂ + 50 mM TBABr was purged with N₂ for 10 min prior to each measurement. Scans were performed at 5 mV s⁻¹ from 0 V to -1.2 V versus the reference and the second CV sweep is plotted.

For two-electrode CV experiments, a full pouch cell was scanned at 10 mV s⁻¹ from 0 V to 1.8, 1.9, and 2.0 V.

Permeability test. To measure the permeability of the CBPE, a piece of the film (1.13 cm² exposed area) was placed in the center of an H-cell to separate 7 mL of water on one side from 7 mL of 1 M aqueous HBr solution on the other. The pH of the water was measured over time with a Fisherbrand™ Accumet™ pH probe calibrated with pH 4, 7, and 10 buffer solutions. Measurements taken at 0, 12, 24, 48, and 72 h are reported in Table S2 along with experimental controls. The experiment was repeated with 130-μm-thick expanded graphite foil (EG) for a reference. The results are summarized in Figure S3.

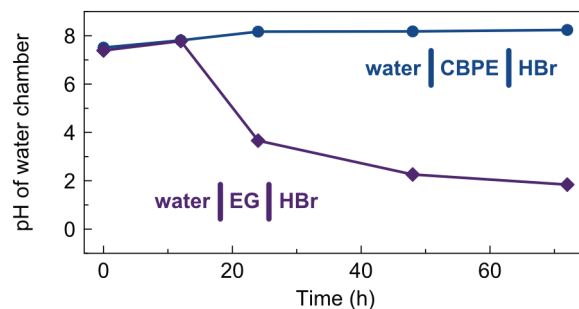


Fig. S3. Permeability test of CBPE film. The measured pH versus time for a reservoir of water separated from 1 M HBr by a piece of the CBPE film in an H-cell is shown. No decrease in the pH of the water is measured over 72 h, indicating negligible diffusion of the HBr electrolyte across the impermeable CBPE. A slight increase in pH at the beginning of the test is observed and separate control vials with only water and with water + CBPE exhibit the same behavior (see Table S2). Repeating the experiment with expanded graphite (EG) instead of CBPE results in a rapid decrease of the pH, suggesting that EG is much more permeable to the aqueous HBr electrolyte.

Table S2. Change in pH over time of water separated from 1 M aq. HBr by CBPE and EG films

Elapsed Time	0 h	12 h	24 h	48 h	72 h
Control 1: pH of water in a vial	7.51	7.89	8.10	8.19	8.30
Control 2: pH of water + CBPE in a vial	7.51	7.90	8.12	8.19	8.28
Result: pH of water in the H-cell separated from 1 M aq. HBr by CPBE	<u>7.51</u>	<u>7.81</u>	<u>8.17</u>	<u>8.18</u>	<u>8.24</u>
Control 1: pH of water in a vial	7.39	8.05	8.16	8.14	8.12
Control 2: pH of water + EG in a vial	7.39	8.03	8.07	8.12	8.22
Result: pH of water in the H-cell separated from 1 M aq. HBr by EG	<u>7.39</u>	<u>7.78</u>	<u>3.66</u>	<u>2.26</u>	<u>1.84</u>

Carbon electrodes. For the preparation of electrodes, activated carbon (Norit[®] A-Supra), polytetrafluoroethylene (PTFE) binder (60 weight % aqueous dispersion from Sigma-Aldrich), and acetylene black conductive additive (Vulcan[®] XC72R) were mechanically mixed in a 90:5:5 mass ratio with isopropanol, and the resulting slurry was repeatedly rolled and folded with a

PTFE rolling pin. This mass was then rolled between sheets of PET plastic into a single freestanding film with a thickness of $265 \pm 15 \mu\text{m}$ with an Emporio[®] Pasta Machine. Electrodes were cut from the film and dried overnight at $175 \text{ }^\circ\text{C}$ in air, and then dried under high vacuum at room temperature for two days.

ZnBr₂ electrolyte. The electrolyte prepared for the cells in this work was 5 M ZnBr₂ + 1 M NaBr. To suppress dendrite formation, poly(ethylene glycol) (PEG, M.W. = 200) additive was included at 4.5% v/v.³

Cell Design, Assembly, and Electrochemical Performance Measurements

Pre-adsorption of TBABr complexing agent. TBABr does not dissolve in the ZnBr₂/NaBr electrolyte because tetrabromozincate anions, $[\text{ZnBr}_4]^{2-}$, will form and precipitate as an insoluble complex with TBA⁺ out of solution.⁴ To solve this problem, the TBABr complexing agent is pre-adsorbed to the activated carbon by soaking the electrode in a solution of 0.25 M TBABr in the absence of ZnBr₂ (Fig. S4). The electrodes are submerged in this solution for 4 h while vacuum and N₂ (150 psi) are alternately applied to infiltrate the hydrophobic carbon electrodes.

ZnBr₂ pouch cell assembly. After the TBABr pre-adsorption/soaking step, the wet electrode is placed in contact with a paper separator that has been saturated with a fixed volume of the ZnBr₂/NaBr electrolyte. The full cell assembly consists of the activated carbon positive electrode, a 180- μm -thick paper separator, and a plastic spacer between two CBPE current collectors. This cell assembly is heat-sealed to form a pouch (Fig. S5 and S6) and left to rest for 12 h before cycling/performance tests. As the ZnBr₂ diffuses into the electrode during this period, the TBA-bromozincate complex forms and adsorbs to the activated carbon surface (Fig. S4). This mixing of the electrolyte with the aqueous TBABr solution in the electrode dilutes the ZnBr₂ electrolyte, decreasing the concentration from the initial 5 M in the separator to $\sim 2.5\text{-}3 \text{ M}$ in the final assembled cell.

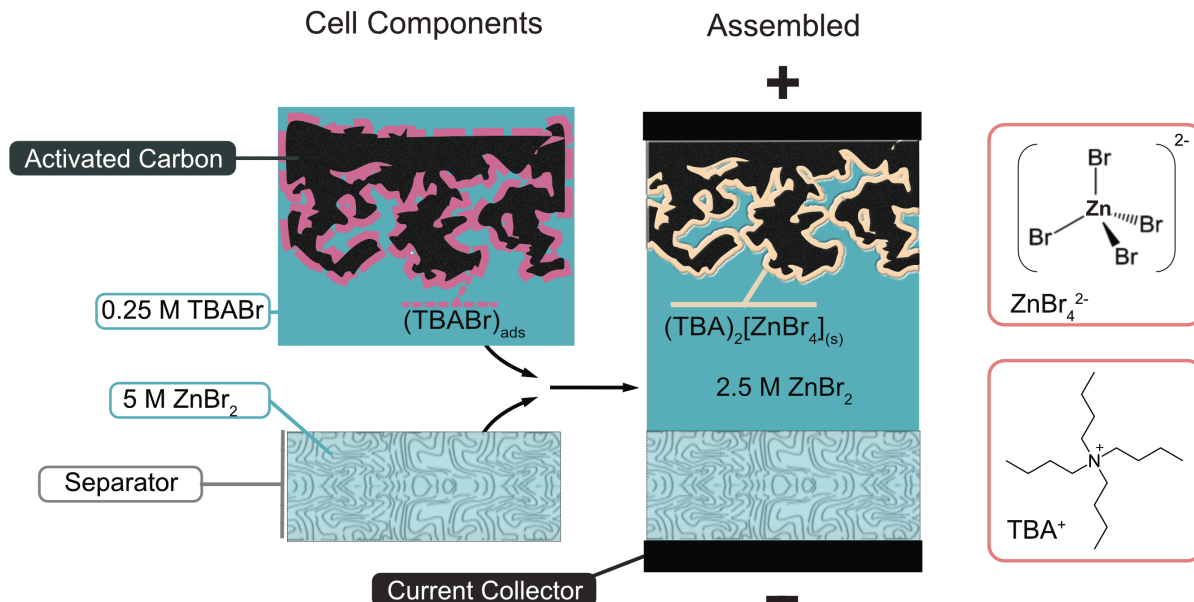


Fig. S4 Zinc-bromine cell construction. The activated carbon electrode is pre-soaked in a TBABr solution to pre-adsorb the Br₃⁻ complexing agent at the surface. Separately, the paper separator is wet with a fixed volume of the ZnBr₂ electrolyte. When the electrode is placed in contact with the separator in a cell assembly, bromozincate anions complex with TBA⁺ and precipitate. This procedure ensures that both the complex and the TBA⁺ it contains are retained in the high-surface-area pores of the electrode. Although not shown, the ZnBr₂ electrolyte contains NaBr and poly(ethylene glycol), as discussed in the previous section.

Pouch preparation. To prepare the heat-sealed pouches, square pieces of CBPE current collector (Linqstat XVCF), paper separator (WhatmanTM #1), and polyethylene spacer (90- μ m-thick plastic bag) are cut according to the dimensions in Table S3.

After the pouch cell materials are cut, cell assembly is completed with a commercial heat sealer (KF-305 hand sealer, 12" \times 5 mm) with the following steps:

1. The plastic spacer is heat-sealed to all four edges of the negative CBPE CC. The paper separator is trapped between these layers at its edges and held in position laterally by the sealed edges (Fig. S5a).
2. The positive CBPE CC is then heat-sealed to the other side of the plastic spacer on one edge to create a flexible flap (Fig. S5b).

- After adding ZnBr_2 electrolyte to the paper separator and placing the TBABr-soaked electrode on top of the separator, the flap is closed and the remaining three edges are sealed (Fig. S5c).

Table S3. Dimensions of the components used for different pouch geometries

	Individual Pouch (Fig. 5)	Scaled Bipolar Stack (Fig. 6)
Electrode	1.0 cm × 1.0 cm	2.5 cm × 2.5 cm
Plastic Spacer	Outer: 3 cm × 3 cm Inner: 1.1 cm × 1.1 cm	Outer: 4.5 cm × 4.5 cm Inner: 2.54 cm × 2.54 cm
Separator	1.27 cm × 1.27 cm	3 cm × 3 cm
CBPE CC	2.5 cm × 2.5 cm	4 cm × 4 cm
Electrolyte*	35 μL	195 μL (per cell)

*This represents the quantity of ZnBr_2 electrolyte added directly to the dry separator. Due to the additional aqueous TBABr solution in the positive electrode, the total electrolyte volume is ~60% higher after assembly.

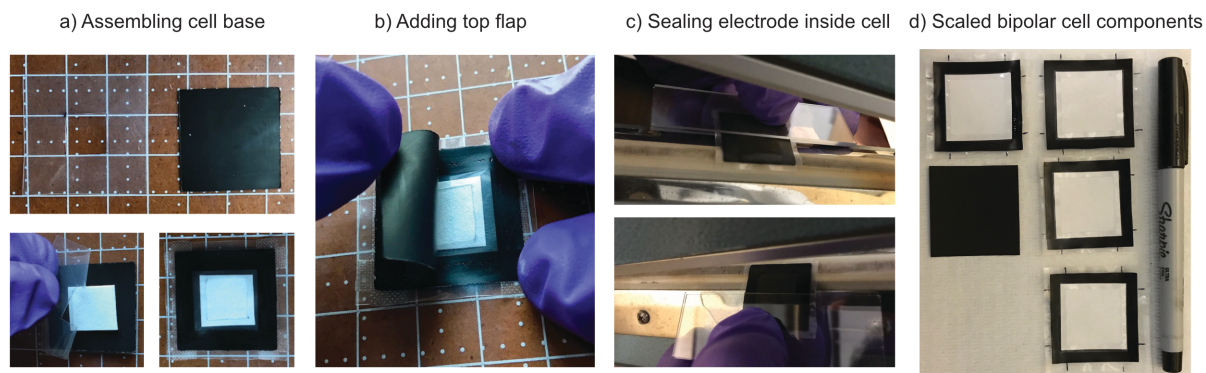


Fig. S5 Assembly of pouch cells. (a) The plastic spacer is heat-sealed to all four edges of the negative CBPE CC. (b) The positive CBPE CC is heat-sealed to the other side of the plastic spacer on one edge to create a flexible flap. (c) After adding ZnBr_2 electrolyte and the positive electrode, the flap is closed and the remaining three edges are sealed. (d) Current collectors prepared for the scaled bipolar pouch before assembly. A negative CC/plastic spacer assembly (top left), positive CC (middle left), and three bipolar CC/plastic spacer assemblies (right) are shown. The markings on the plastic spacers are to assist with alignment.

For bipolar current collectors, instead of sealing a single CBPE CC onto the top of the pouch in Step 2, the new layer that becomes the flap is another CBPE CC/plastic spacer assembly, identical to that prepared in Step 1. In the scaled bipolar pouch cell, for example, there are four identical CBPE/plastic spacer assemblies before assembly (one negative CC and 3 bipolar CCs) and one CBPE positive CC (Fig. S5d). For each new cell added to the top of the stack, Steps 2 and 3 are repeated.

Test configuration. In order to test individual pouch cells, the sealed pouch was placed between two rigid endplates (Fig. S6). The endplates consist of aluminum tape stuck to a glass plate. To improve electrical contact between the aluminum foil and the pouch, the metal is roughened with sandpaper and coated with a thin layer of conductive carbon assembly paste (MG Chem 847-25ML). Pressure is then applied to the full assembly using a pair of small ($\frac{3}{4}$ ") binder clips, and the leads are clipped to the protruding aluminum tape before cell cycling.

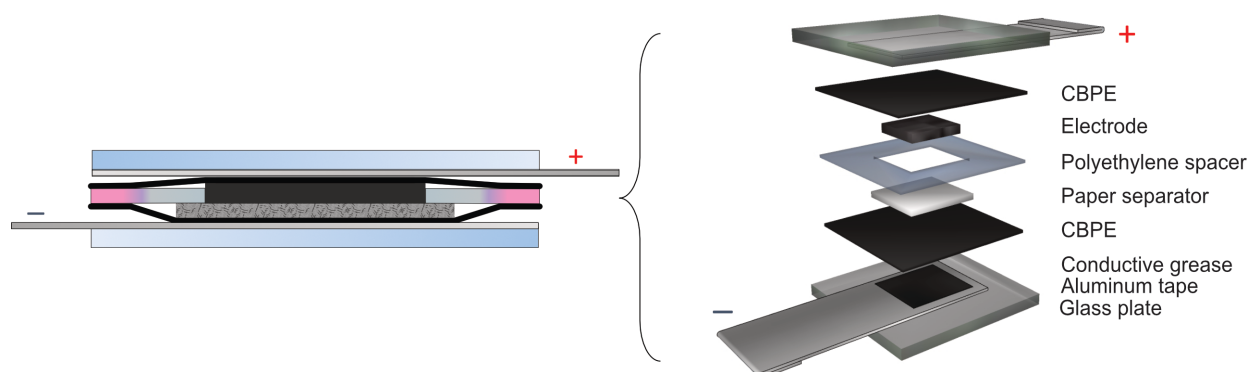


Fig. S6 Testing setup for pouch cells. The heat-sealed pouch is placed between glass plates covered in aluminum tape and a carbon conductive paste. External pressure is applied to the entire assembly by a pair of steel binder clips (not shown) acting as compressive springs.

For the scaled bipolar pouch, a similar procedure was followed. As shown in the manuscript (Fig. 6d), titanium plates were used as endplates instead of aluminum tape on glass.

The metal plates were again roughened and covered in conductive carbon paste, and four steel binder clips were used to apply pressure to the stack.

Electrochemical characterization of pouch cells. All galvanostatic charge/discharge (GCD) cycling tests were performed at a temperature of 25 ± 1 °C on a Bio-logic VMP3 potentiostat/galvanostat. The applied current for GCD cycling tests was normalized to the dry mass (activated carbon, carbon black, and PTFE binder) of the positive electrode. Charging was performed to a capacity limit of 50 mAh g⁻¹, 100 mA h g⁻¹, or 150 mA h g⁻¹. Potential limits were applied for discharging, with V_{\min} values of 1 V for single cells and 5 V for the scaled bipolar stack. The following equations are used for calculating device performance (I = applied current, t = time, and V = voltage):

Charge capacity, Q_{ch} (mA·h)	$Q_{\text{ch}} = I_{\text{ch}} \cdot t_{\text{ch}}$
Discharge capacity, Q_{dis} (mA·h)	$Q_{\text{dis}} = I_{\text{dis}} \cdot t_{\text{dis}}$
Coulombic efficiency, η_{C}	$\eta_{\text{C}} = Q_{\text{dis}}/Q_{\text{ch}}$
Charge energy, E_{ch} (W·h)	$E_{\text{ch}} = \int_0^{t_{\text{ch}}} I_{\text{ch}} \cdot V(t) dt$
Discharge energy, E_{dis} (W·h)	$E_{\text{dis}} = \int_0^{t_{\text{dis}}} I_{\text{dis}} \cdot V(t) dt$
Energy efficiency, η_{E}	$\eta_{\text{E}} = E_{\text{dis}}/E_{\text{ch}}$
Voltage efficiency, η_{V}	$\eta_{\text{V}} = \eta_{\text{E}}/\eta_{\text{C}}$
Average discharge power, P_{dis} (W)	$P_{\text{dis}} = E_{\text{dis}}/t_{\text{dis}}$

Energy and power reported in the text indicate discharge energy (E_{dis}) and average discharge power (P_{dis}) and are normalized on both a gravimetric and volumetric basis. For gravimetric normalization, specific power and energy are calculated based on the mass of the activated carbon positive electrode (including the binder and conductive carbon additive) to be consistent with other similar systems reported in the literature. For volumetric normalization, power and energy density are calculated based on the pouch volume. This volume is calculated

by multiplying the geometric area of the electrode, A , by the thickness of the pouch (electrode + separator + CBPE CCs), d . This neglects the volume occupied by the seal around the perimeter of the pouch, but the volume of this region is small and becomes increasingly negligible as the cell scales to larger sizes.

The self-discharge rate was quantified based on the remaining discharge energy as a function of open circuit time, δ . An open circuit energy efficiency (or energy retention), η_R , is defined as the ratio of the energy retained after time δ at open circuit to the initial discharge energy and calculated by the following formula⁵:

$$\text{Open circuit energy efficiency, } \eta_R \quad \eta_R(\delta) = E_{\text{dis}}(\delta)/E_{\text{dis}}(0)$$

Experimental demonstration of cell balancing. For experimental verification that series-connected ZnBr₂ cells can stay balanced, two individual cells were connected in series and cycled together at 1 A g⁻¹ to a capacity of 100 mA h g⁻¹, as shown in Fig. S16. The cells stayed balanced over 100 cycles, with each cell completing the faradaic plateau at the end of every discharge. The cycling test was then repeated with the cells deliberately offset, where Cell A was initially fully discharged and Cell B was pre-charged to 50 mA h g⁻¹. When the two cells were reconnected in series and cycled normally, Cell B would overcharge on each subsequent cycle to ~150 mA h g⁻¹ (and only discharge back to ~50 mA h g⁻¹) while Cell A would operate normally between 0 and 100 mA h g⁻¹ (Fig. S16c). Although the total voltage profile for the 2 cells in series (orange) appears relatively unchanged after the offset, the individual cells deviate significantly from their normal profiles (Fig. S16b). Over the course of 50 cycles (represented as 101st to 150th cycles in Fig. S16c), however, the cells re-balanced, the potential profiles returned to their initial equilibrium state, and cycling continued normally, indicating that the self-balancing chemistry in the ZnBr₂ system is effective.

Supplementary Data and Figures

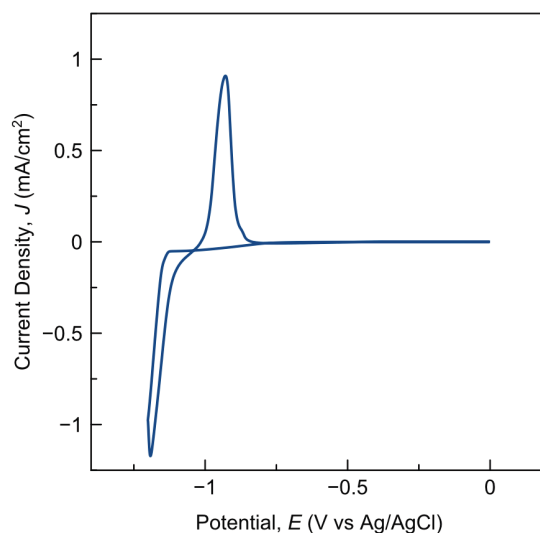


Fig. S7. Cyclic voltammogram of zinc plating and stripping. CV of 0.1 M ZnBr₂ + 50 mM TBABr from 0 V to -1.2 V at a scan rate of 5 mV s⁻¹ on a CBPE working electrode. A Pt wire served as the counter electrode and an Ag/AgCl reference electrode was used. This result shows that Zn metal is reversibly plated on the CPBE working electrode.

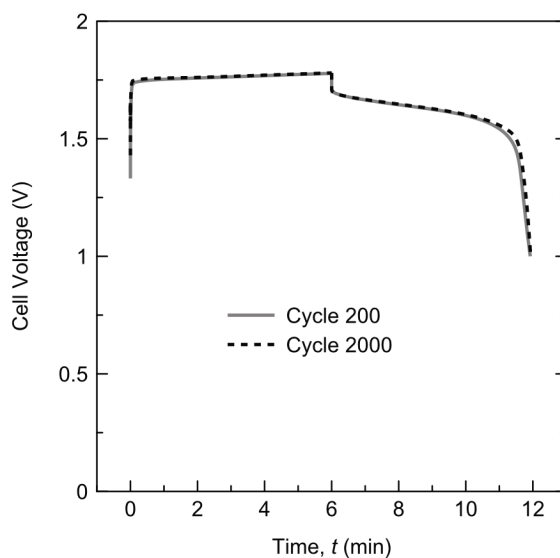


Fig. S8. Voltage profile before and after long-term cycling. GCD profiles of a ZnBr₂/TBABr/CBPE cell for the 200th and 2000th cycle during the long-term stability test at a rate of ± 1 A g⁻¹ charged to 100 mA h g⁻¹. These results indicate that after extended cycling there is no significant change in the charge/discharge plateaus or in the cell *IR*-drop.

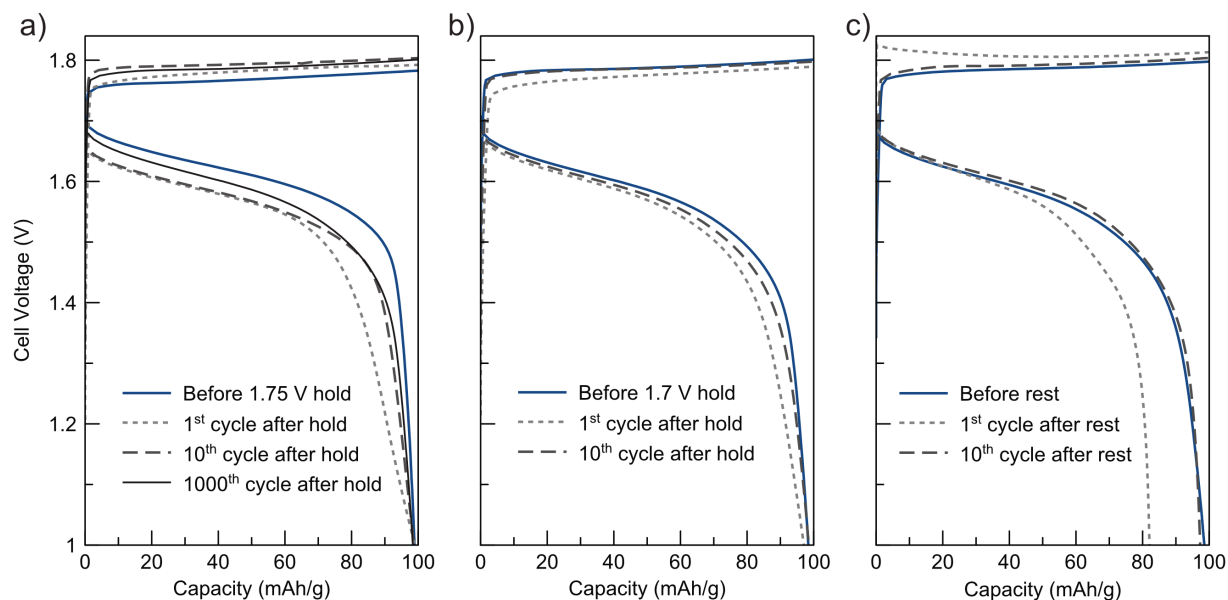


Fig. S9. Stability tests after voltage holds and rests. GCD profiles at $\pm 1 \text{ A g}^{-1}$ for a $\text{ZnBr}_2/\text{TBABr}/\text{CBPE}$ cell before and after (a) holding the cell at 1.75 V for 50 h, (b) holding the cell at 1.7 V for 100 h, and (c) leaving the cell at rest in the fully discharged state for one week. The discharge profiles immediately following the 1.75 V hold and the 1.7 V hold deliver a capacity of 228 and 107 mAh g^{-1} , respectively. The internal resistance of the cell increases after the 1.75 V hold and partially recovers with continued cycling, while the 1.7 V hold results in only minor changes to the GCD profile. After the one-week rest the cell has a high overpotential at the beginning of the charge and a low Coulombic efficiency on the discharge, but quickly returns to normal charging/discharging behavior. These data show that the cell performance is largely insensitive to both high-voltage overcharging as well as resting in the discharged state.

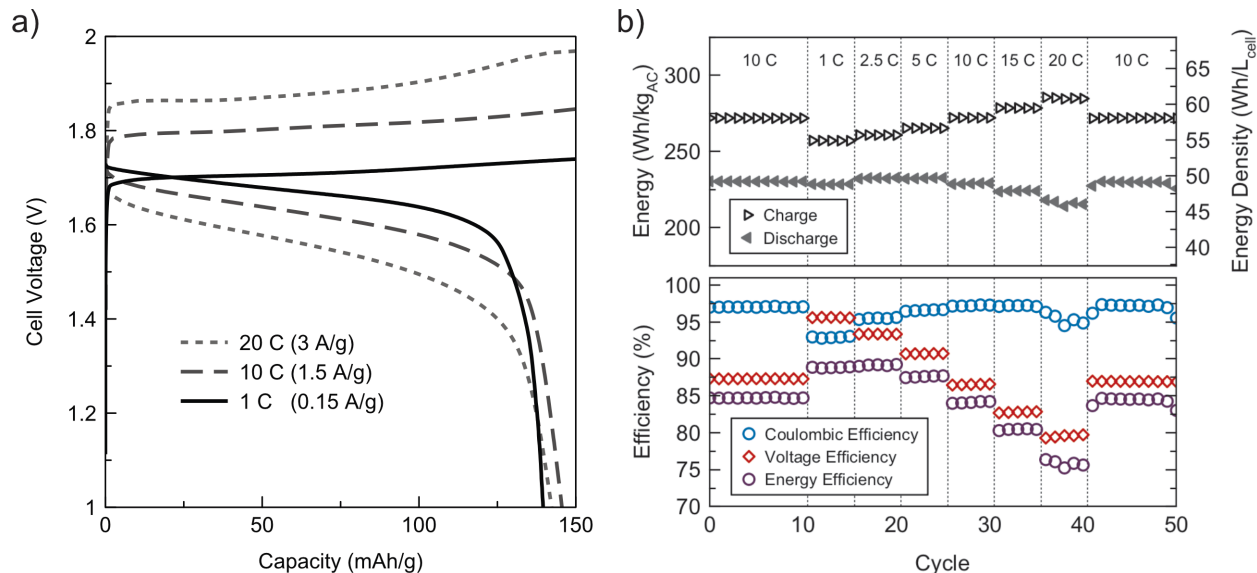


Fig. S10 Electrochemical performance data for CPBE pouch cell charged to 150 mA h g^{-1} .
 a) Typical galvanostatic potential profiles for a $\text{ZnBr}_2/\text{TBABr}/\text{CBPE}$ cell at different charge/discharge rates. The resulting flat charge/discharge plateaus are characteristic of the zinc-bromine cell chemistry. b) Charge and discharge energy as well as Coulombic, voltage, and energy efficiency at different rates for a $\text{ZnBr}_2/\text{TBABr}/\text{CBPE}$ cell. The cell is charged to 150 mA h g^{-1} and energies are normalized to the mass of the activated carbon electrode (left axis) and to the full cell volume (right axis), which includes the electrode, separator, and CBPE current collectors. Note that at high charging rates of 20 C, the cell shows unusual behavior in both the GCD potential profile and in the Coulombic efficiency.

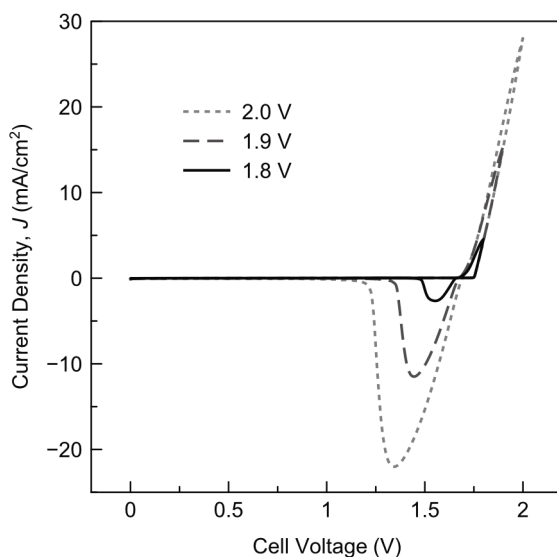


Fig. S11 Cyclic voltammograms of a full ZnBr₂/TBABr/CBPE cell. Two-electrode CVs of a pouch cell at a scan rate of 10 mV s⁻¹ from 0 V to 1.8, 1.9, and 2.0 V. These data show the primarily faradaic response of the redox electrolyte and are consistent with the GCD profiles.

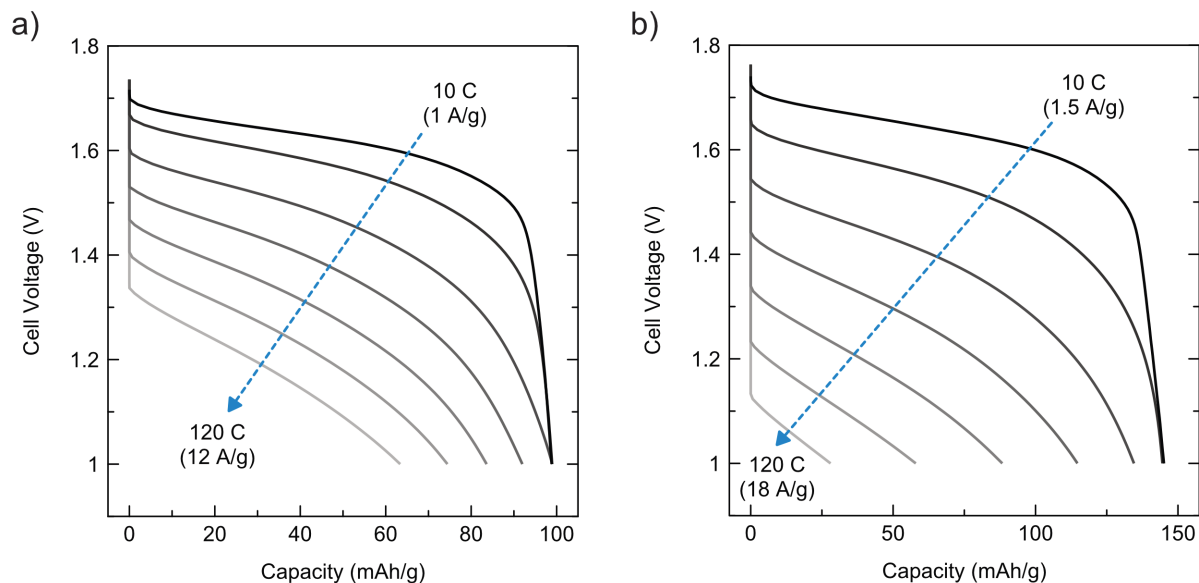
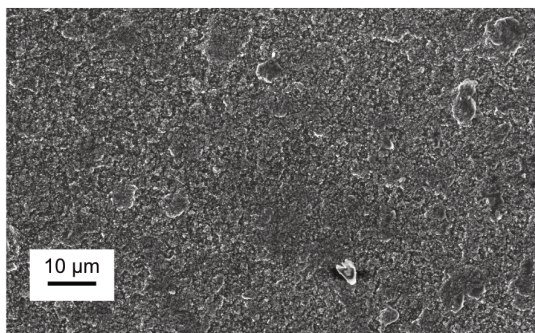
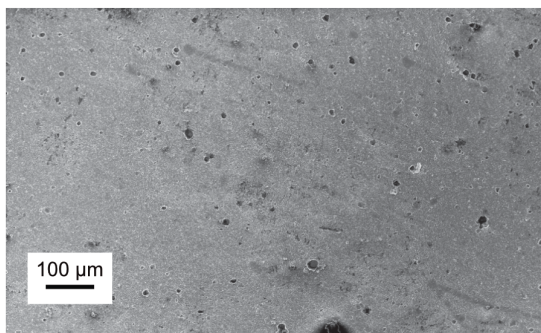


Fig. S12 High-rate galvanostatic discharge profiles. Potential profiles from discharge rate tests where the cell was charged only at a single rate of 10 A g⁻¹ (1 C) to a capacity of (a) 100 mA h g⁻¹ or (b) 150 mA h g⁻¹ and discharged at different rates (10 C, 15 C, 20 C, 40 C, 60 C, 80 C, 100 C, and 120 C) to a potential of 1 V.

a) Pristine CBPE film



b) CBPE after 16 days in pure Br₂

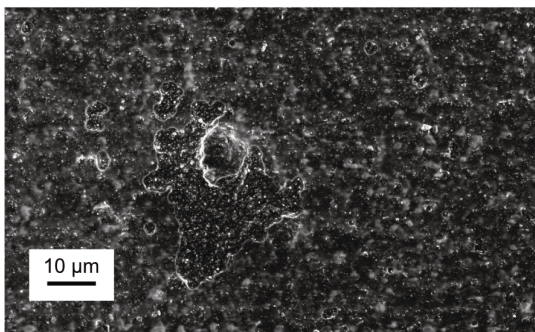
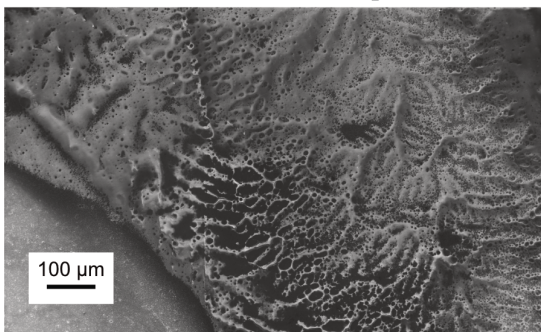
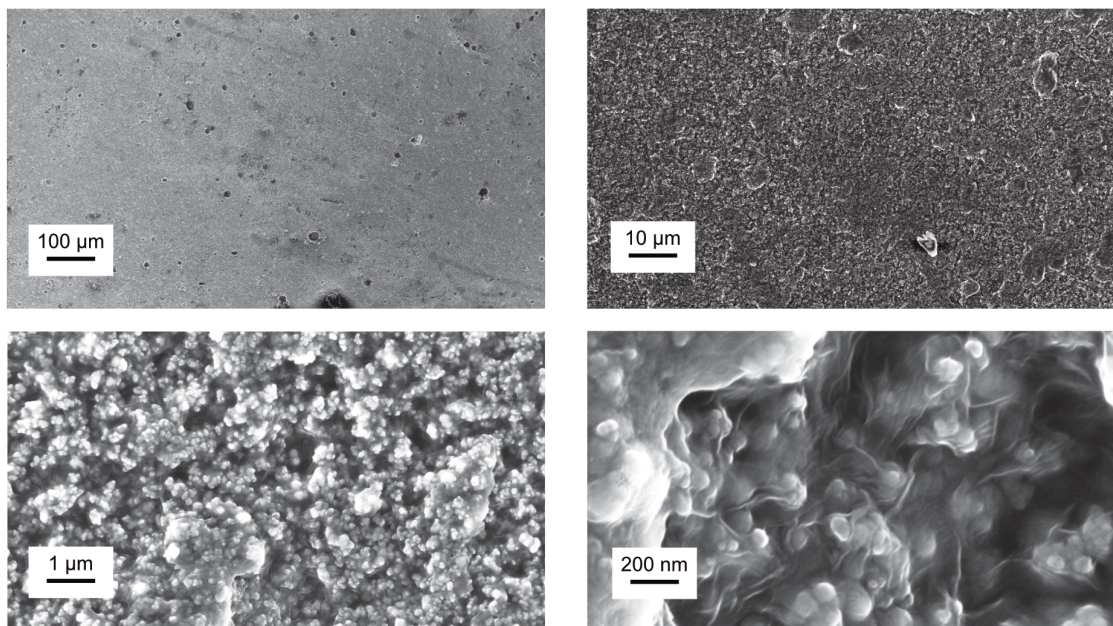


Fig. S13 SEM micrographs of CBPE film (a) in pristine condition and (b) after soaking 16 days in pure Br₂. These data show that in the absence of complexing agents, the surface of the CBPE is affected by the corrosive redox electrolyte. Micrographs were produced using an FEI Nova NanoSEM 650 and a Zeiss Ultra-55 SEM.

a) Pristine CBPE film



b) CBPE from cell cycled 1500 times

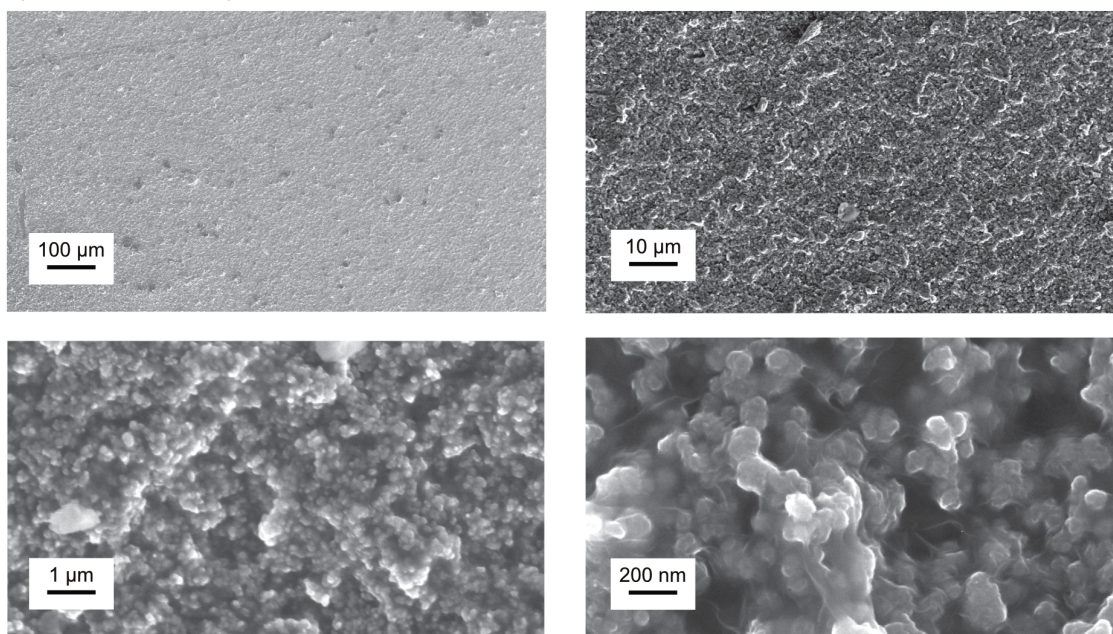


Fig. S14 SEM micrographs of CBPE film (a) in pristine condition and (b) after serving as a positive current collector in a $\text{ZnBr}_2/\text{TBABr}/\text{CBPE}$ pouch cell for 1500 cycles. These data show that the surface of the CBPE has minimal damage after operating in a cell. The cell environment with aqueous electrolyte and TBA acting as a strong bromine complexing agent is therefore less aggressive than pure bromine (Fig. S13).

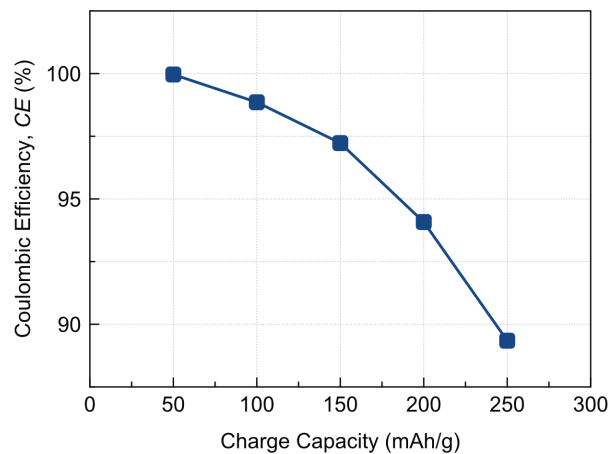


Fig. S15 Coulombic efficiency versus charging capacity. A $\text{ZnBr}_2/\text{TBABr}$ pouch cell was cycled at 1 A g^{-1} to different capacity limits in 50 mA h g^{-1} increments. Coulombic efficiency decreases substantially when the cell is overcharged, due to a finite quantity of TBABr complexing agent.

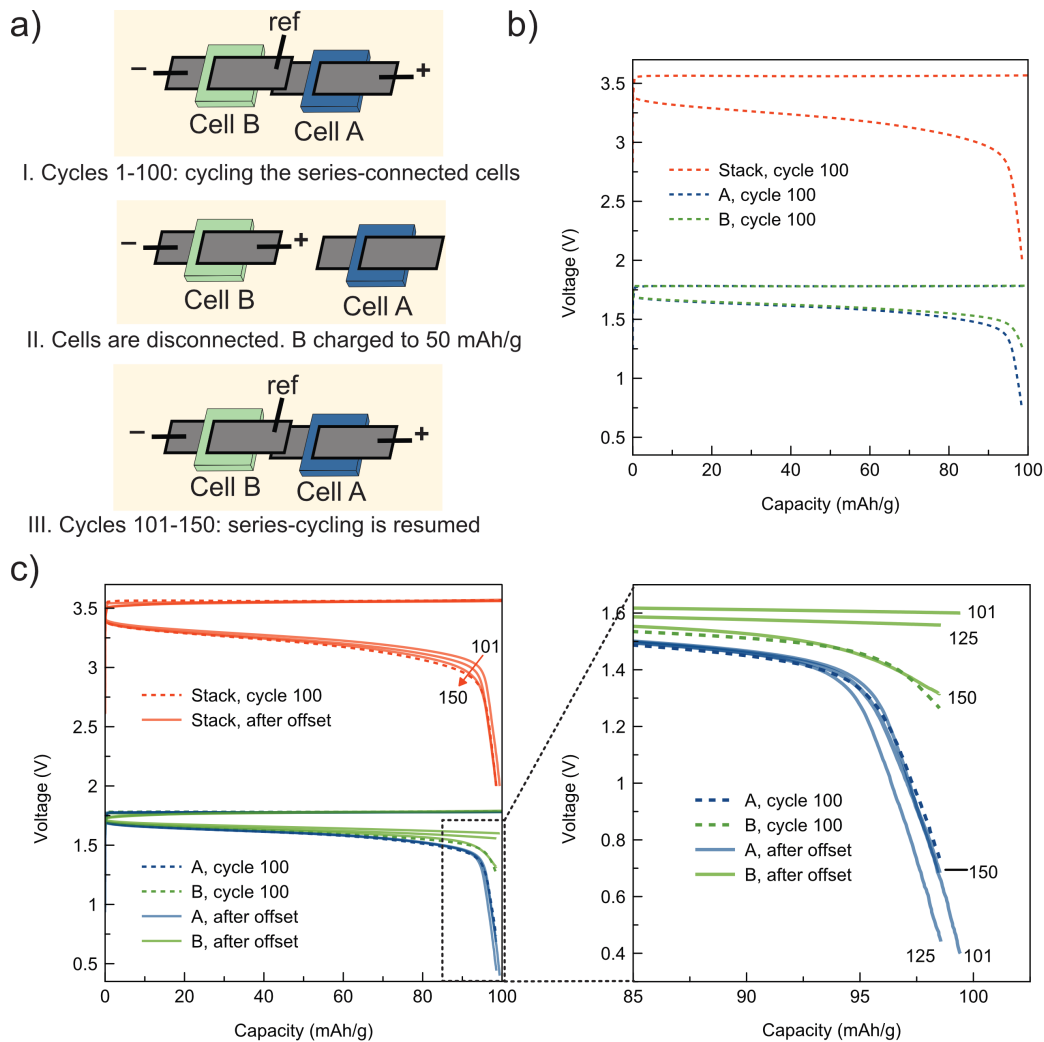


Fig. S16 Self-balancing of series-connected ZnBr_2 cells. (a) Schematic illustrating the experiment in which two cells, A and B, are cycled in series while the stack voltage is measured. The reference lead (ref) at the Cell A/Cell B junction enables the individual cell potentials to be measured. The stack is charged to 100 mA h g^{-1} and discharged to 2 V for 100 cycles. After the initial cycles, the cells are deliberately offset so that Cell A is initially fully discharged and Cell B is pre-charged to 50 mA h g^{-1} . This creates a condition where Cell B overcharges on each subsequent cycle once the cells are reconnected. The cells can rebalance after the offset due to increased internal self-discharge in Cell B from the redox shuttle. (b) The GCD profile is shown for Cell A, Cell B, and the series A/B stack for the 100th cycle (dashed lines). Cells A and B reach different voltages on the discharge due to both cells being charged to the same capacity despite Cell B having a 7.5% larger electrode. (c) The solid lines indicate the 1st, 25th and 50th cycles after the cells are intentionally offset and cycling is resumed. The zoomed area for the GCD profiles of Cell A and Cell B shows that Cell A overdischarges and Cell B cannot complete its discharge plateau after the offset. The profiles gradually re-converge (note 150th cycle overlaps with the 100th cycle) due to self-balancing in the cell stack.

References

- 1 S. Gheyhani, Y. Liang, Y. Jing, J. Q. Xu and Y. Yao, *J. Mater. Chem. A*, 2016, **4**, 395.
- 2 N. Blomquist, T. Wells, B. Andres, J. Bäckström, S. Forsberg and H. Olin, *Sci. Rep.*, 2017, **7**, 1–7.
- 3 S. J. Banik and R. Akolkar, *J. Electrochem. Soc.*, 2013, **160**, D519–D523.
- 4 M. E. Easton, P. Turner, A. F. Masters and T. Maschmeyer, *RSC Adv.*, 2015, **5**, 83674–83681.
- 5 S.-E. Chun, B. Evanko, X. Wang, D. Vonlanthen, X. Ji, G. D. Stucky and S. W. Boettcher, *Nat. Commun.*, 2015, **6**, 7818.